Inorganic Chemistry Communications 132 (2021) 108847

Contents lists available at ScienceDirect

Inorganic Chemistry Communications

journal homepage: www.elsevier.com/locate/inoche

A novel berberine-based colorimetric and fluorometric probe for Hg^{2+} detection and its applications in water samples

Shutang Ruan [a], Yan Zhang [a], Suzhen Wu [b], Yu Gao [a], Lijuan Yang [a], Mingxin Li [a], Yiqin Yang [a], Zhonglong Wang [a,*], Shifa Wang [a,*]

[a] Co-Innovation Center of Efficient Processing and Utilization of Forest Resources, College of Chemical Engineering, College of Light Industry and Food, Nanjing Forestry University, Nanjing 210037, China
[b] School of Basic Medicine, Gannan Medical University, Ganzhou 341000, China

ARTICLE INFO

Keywords:
Berberine
Fluorescent probe
Colorimetric probe
Hg^{2+} detection

ABSTRACT

The development of small molecule fluorescent probes for detection of heavy metal ions is highly desirable in fluorescent sensors area, and mercury (Hg^{2+}) is a heavy metal pollutant in environment and food chain processes. Herein, we reported the design and synthesis of a novel berberine-based fluorescent probe **P1**, which can specifically recognize Hg^{2+} in CH_3OH/PBS (8:2, *v/v*, pH = 7.4, 10 mM) solution by the colorimetric and fluorometric changes. The probe **P1** displayed high selectivity, superior sensitivity and fast response toward Hg^{2+} with a low detection limit and a wide range of pH values. This probe can provide a convenient and effective way for Hg^{2+} detection on test paper strips. Moreover, the probe **P1** can be applied to quantitatively detect Hg^{2+} in real environmental water samples.

1. Introduction

Hg^{2+} is a high toxic heavy metal pollutant and widely distributes in water and soil [1–3]. Excessive Hg^{2+} in the bodies easily causes some serious diseases, such as kidney damage [4], minamata disease [5], endocrinium and nervous system damage [6], cognitive and motor disorders [7]. It is necessary to control the content of Hg^{2+} in environmental and agricultural products within safe limits [8].

During the past two decades, many chemical analysis methods have been used for detecting toxic heavy metal, such as atomic absorption spectroscopy [9], high resolution ICP-MS [10], spectrophotometry [11] and fluorescent probe technique [12–15]. Among these detection methods, fluorescent probe technique has been widely accepted owing to its on-site detection, real-time analysis, high sensitivity, low cost and fast response. Recently, a number of fluorescent probes have been reported for detecting Hg^{2+} in real samples and living cells. However, some probes were based on "turn-off" mechanism through the spin–orbit coupling effect which cause fluorescence quenching [16–18]. Therefore, the fluorescent probes for detecting Hg^{2+} based on "turn-on" mechanism have attracted more and more attentions [19–22].

Berberine is a kind of typical isoquinoline alkaloids extracted from huanglian (*Rhizoma coptidis*) [23], and its derivatives were widely used as anti-bacterial agent [24], antiviral agent [25–27], antioxidant and anticancer [28,29]. In addition, it is a valuable researching direction of fluorescence-based theranostics based on berberine for effective diagnosis and therapy in cancer cells [30].

In our previous work [31], a dual-functional fluorescent probe for the detection of both Hg^{2+} and ClO^- has been designed and synthesized from berberine. In order to further expand the application of berberine and detect Hg^{2+} by the naked eye and fluorescence conveniently. Herein, based on the desulfurization reaction of the mercaptal group, a dual-mode berberine-based colorimetric and fluorometric probe was designed and synthesized for the recognization of Hg^{2+}. Meanwhile, the probe **P1** showed "turn-on" fluorescent response toward Hg^{2+} recognition in real water samples. Moreover, from the fluorescence detection experiments, the probe **P1** exhibited fast response, wide pH range, lower detection limit, high selectivity and sensitivity.

2. Experimental

2.1. Instruments and materials

All chemicals and solvents were purchased from commercial sources and used without further purification. ^1H NMR and ^{13}C NMR spectra

* Corresponding authors.
E-mail addresses: wang_zhonglong@njfu.edu.cn (Z. Wang), wangshifa65@163.com (S. Wang).

https://doi.org/10.1016/j.inoche.2021.108847
Received 19 June 2021; Received in revised form 23 July 2021; Accepted 5 August 2021
Available online 8 August 2021

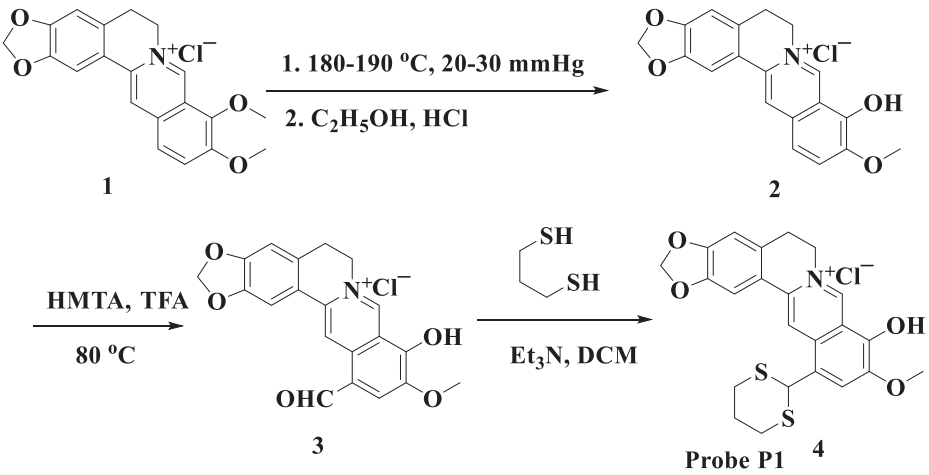

Scheme 1. Synthesis of probe **P1**.

were recorded on a Bruker AV 400 spectrometer in DMSO-d_6 and tetramethylsilane (TMS) as internal standard. High-resolution mass spectra (HRMS) were tested by an America Agilent 5975c mass spectrometer. UV–vis absorption spectra were recorded by a Shimadzu UV-2450 at the room temperature. Fluorescence spectra were carried out on fluorescence spectrophotometer (LS 55, Perkin Elmer).

2.2. Synthesis of probe *P1*

As shown in Scheme 1, berberine was selectively demethylated under vacuum and heating conditions, and then acidized and formylated to get compound **3**. The probe **P1** was obtained by condensation of compound **3** with 1,3-propanedithiol. The chemical structure of the above compounds and probe **P1** was characterized by ^{1}H NMR and HR-MS (Fig. S1-S7).

2.2.1. Synthesis of compound *2*

Berberine chloride (10.0 g, 26.9 mmol) was heated at 180–190 °C for 30–60 min under vacuum to afford dark wine solid, which was washed with MeOH (80 mL) and filtered to afford the red compound. And this crude product was added C_2H_5OH (100 mL) and HCl (3.0 M, 70 mL) to stir for 6 h to obtain yellow material, which was washed with CH_3OH/Et_2O (v/v = 3:1) 3 times (3 × 60 mL) to afford compound **2** as a yellow solid, 8.87 g, yield: 92.4%. ^{1}H NMR (400 MHz, DMSO-d_6) δ: 11.31 (s, 1H), 9.97 (s, 1H), 8.88 (s, 1H), 8.12 (d, J = 8.9 Hz, 1H), 7.82 (s, 1H), 7.75 (d, J = 8.9 Hz, 1H), 7.10 (s, 1H), 6.21 (s, 2H), 4.96 (t, J = 6.3 Hz, 2H), 4.09 (s, 3H), 3.25 (t, J = 6.3 Hz, 2H);^{13}C NMR (100 MHz, DMSO-d_6) δ: 149.58, 147.61, 145.70, 145.30, 143.75, 136.52, 132.39, 130.33, 125.43, 120.56, 119.80, 118.03, 117.58, 108.32, 105.29, 101.94, 56.99, 54.89, 26.48;ESI-MS (m/z): $[M-Cl]^+$: calcd. for $C_{19}H_{16}ClNO_4$-Cl^-, 322.1074; found, 322.1074.

2.2.2. Synthesis of compound *3*

Compound **3** was obtained according to the reported procedures [31]. Compound **2** (1.0 g, 3.1 mmol) and hexamine (1.26 g, 9.0 mmol) were dissolved in trifluoroacetic acid (18 mL), and reacted for 8 h at 85 °C. The reaction system was cooled to room temperature, and 3.0 M HCl (15 mL) was added to react at 85 °C for another 2 h. The reacted mixture was immediately poured into ice water, and extracted with ethyl acetate (3 × 30 mL). The combined organic phase was washed with distilled water and brine until neutrality, and then evaporated to remove off the solvent. The residue was purified by silica gel chromatography (CH_2Cl_2/CH_3OH, 10:1, v/v) to give compound **3** as a yellow solid, 0.38 g, yield: 34.6%. ^{1}H NMR (400 MHz, DMSO-d_6) δ: 10.19 (s, 1H), 9.28 (s, 1H), 9.08 (s, 1H), 7.72 (s, 1H), 7.56 (s, 1H), 7.02 (s, 1H), 6.15 (s, 2H), 4.60 (t, J = 6.3 Hz, 2H), 3.77 (s, 3H), 3.10 (t, J = 6.4 Hz, 2H), 1.24 (s, 1H) ;ESI-MS (m/z): $[M-Cl]^+$: calcd. for $C_{20}H_{16}ClNO_5$-Cl^-, 350.1023; found, 350.1049.

2.2.3. Synthesis of compound *4*

Compound **3** (50 mg, 0.14 mmol) and 1,3-propanedithiol (45.4 mg, 0.42 mmol) were dissolved in CH_2Cl_2 (20 mL), and a catalytic amount of BF_3·Et_2O (0.04 mL, 0.30 mmol) was added, and the mixture was reacted at room temperature for 15 h under N_2 atmosphere. The reacted mixture was evaporated to remove off solvent, and the residue was purified by recrystallization with CH_3OH/Et_2O (v/v = 2:1) to obtain compound **4** as a red solid, 37.5 mg, yield: 57.3%. ^{1}H NMR (400 MHz, DMSO-d_6) δ: 9.31 (s, 1H), 8.37 (s, 1H), 7.89 (s, 1H), 7.51 (s, 1H), 7.03 (s, 1H), 6.30 (s, 1H), 6.15 (s, 2H), 4.60 (t, J = 6.2 Hz, 2H), 3.81 (s, 3H), 3.30 (s, 2H), 3.10 (t, J = 6.2 Hz, 2H), 2.90 (dt, J = 14.1, 3.5 Hz, 2H), 1.24 (d, J = 3.3 Hz, 2H) ; ESI-MS (m/z): $[M-Cl]^+$ calcd. for $C_{20}H_{16}ClNO_5$-Cl^-, 440.0985; found, 440.1019.

2.3. Spectroscopic measurements of probe *P1*

The absorption and fluorescence detection experiments were done in CH_3OH/PBS (8:2, v/v, pH = 7.4, 10 mM) solution at the room temperature, and the excitation wavelength is 365 nm. The probe **P1** stock solution (2.5 × 10^{-4} M) was prepared in CH_3OH. The test solution was prepared by adding 100 μL stock solution to 10 mL CH_3OH/PBS buffer (8:2, v/v, pH = 7.4, 10 mM). The solutions of various analytes (5.0 × 10^{-4} M) (including Na^+, K^+, Ca^{2+}, Mg^{2+}, Co^{2+}, Al^{3+}, Ni^{2+}, Sn^{2+}, Ag^{2+}, Zn^{2+}, Cu^{2+}, I^-, NO_3^-, AcO^-, $H_2PO_4^{2-}$, S^{2-}) were prepared in deionized water.

2.4. Visualization of Hg^{2+} in solution by test paper

The filter paper was immersed into the CH_3OH solution of probe **P1** (2.5 × 10^{-4} M) and dried in air for 30 min. The treated test papers were immersed in the Hg^{2+} solution with different concentrations (0 μM-500 μM) for 30 min at the room temperature. The fluorescence color changes of filter paper were observed under day light and 365 nm UV light.

2.5. Quantitation of Hg^{2+} contamination in real water samples

The real water samples were respectively taken from Zhangjiang river and Poyang lake, and the real water samples were utilized to prepare CH_3OH solutions (80%, 10 mM). Hg^{2+} solutions with different concentrations (0, 50, 100, 150, 200, 250 μM) were added to the aforesaid two water samples, and the fluorescence intensity of the water samples were measured using a fluorescence spectrophotometer.

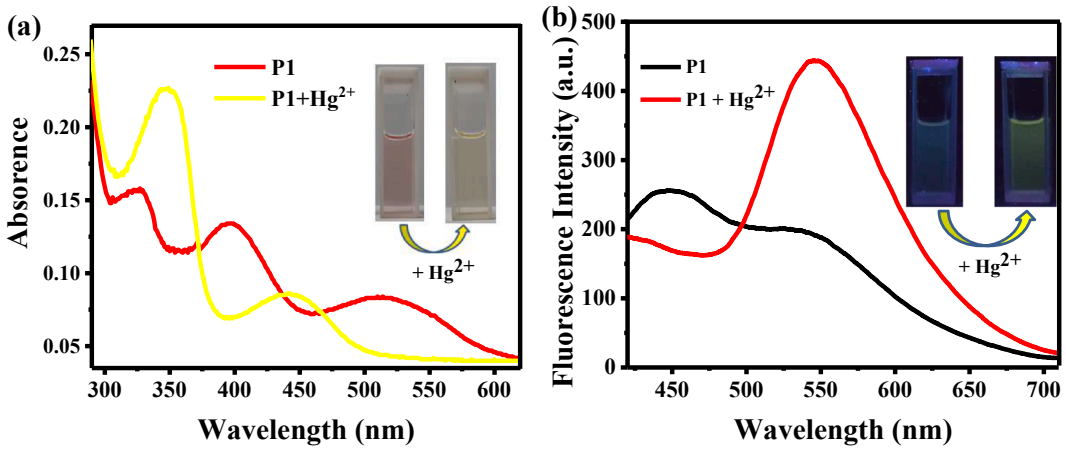

Fig. 1. Absorption (a) and fluorescence emission (b) spectra of probe **P1** (2.5×10^{-4} M) in CH_3OH/PBS (8:2, *v/v*, pH = 7.4, 10 mM) solution in the presence and absence of Hg^{2+} (5.0×10^{-4} M). λ_{ex} = 365 nm. Inset: color changes of probe **P1** solution after the addition of Hg^{2+} under daylight and 365 nm UV-light.

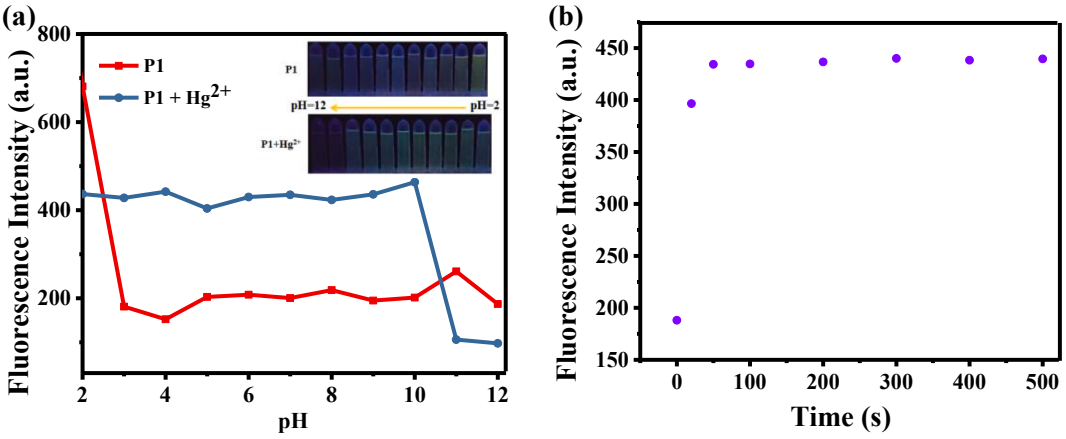

Fig. 2. (a) Fluorescence intensity of **P1** (2.5×10^{-4} M) added to Hg^{2+} (5.0×10^{-4} M) in CH_3OH/PBS (8:2, *v/v*, pH = 7.4, 10 mM) solution from pH = 2.0 to pH = 12.0 at 550 nm. Inset: color changes of **P1** after the addition of Hg^{2+} from pH = 2.0 to pH = 12.0 under 365 nm UV-light. (b) Time-dependent fluorescence spectra of **P1** (2.5×10^{-4} M) presence and absence Hg^{2+} (5.0×10^{-4} M) in CH_3OH/PBS (8:2, *v/v*, pH = 7.4, 10 mM) solution (λ_{em} = 550 nm).

3. Results and discuss

3.1. Spectroscopic properties of probe *P1* to Hg^{2+}

The UV–vis absorbance and fluorescence spectroscopic properties of probe **P1** in the presence and absence of Hg^{2+} at the room temperature were examined. As shown in Fig. 1a, the free probe **P1** showed two absorption peaks at 400 nm and 520 nm. Upon addition of Hg^{2+}, the original maximum absorption peaks were significantly reduced and the new peaks were appeared obviously at 350 nm and 450 nm, and the

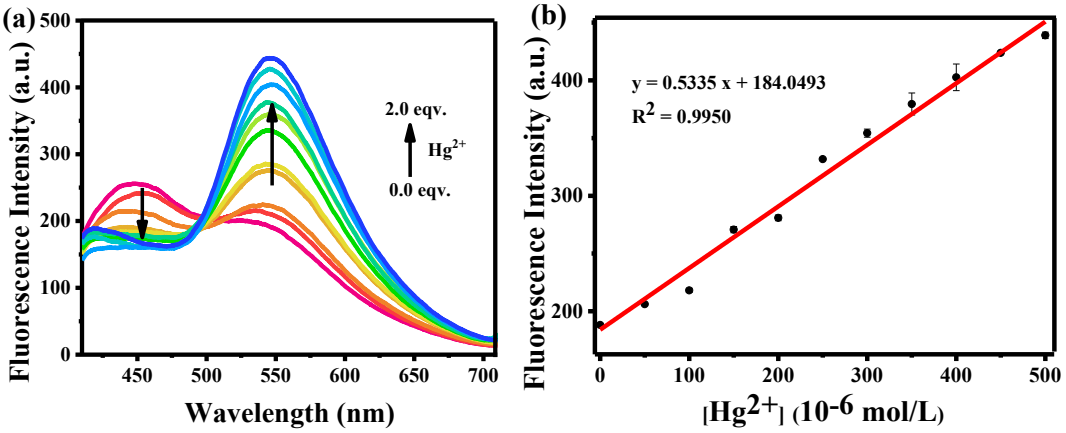

Fig. 3. (a) Fluorescence spectra of **P1** (2.5×10^{-4} M) in the presence of Hg^{2+} (0–2.0 eqv.) in CH_3OH/PBS (8:2, *v/v*, pH = 7.4, 10 mM) solution. (b) Linear calibration curve between the fluorescence intensity of **P1** and Hg^{2+} (0–2.0 eqv.) at 550 nm.

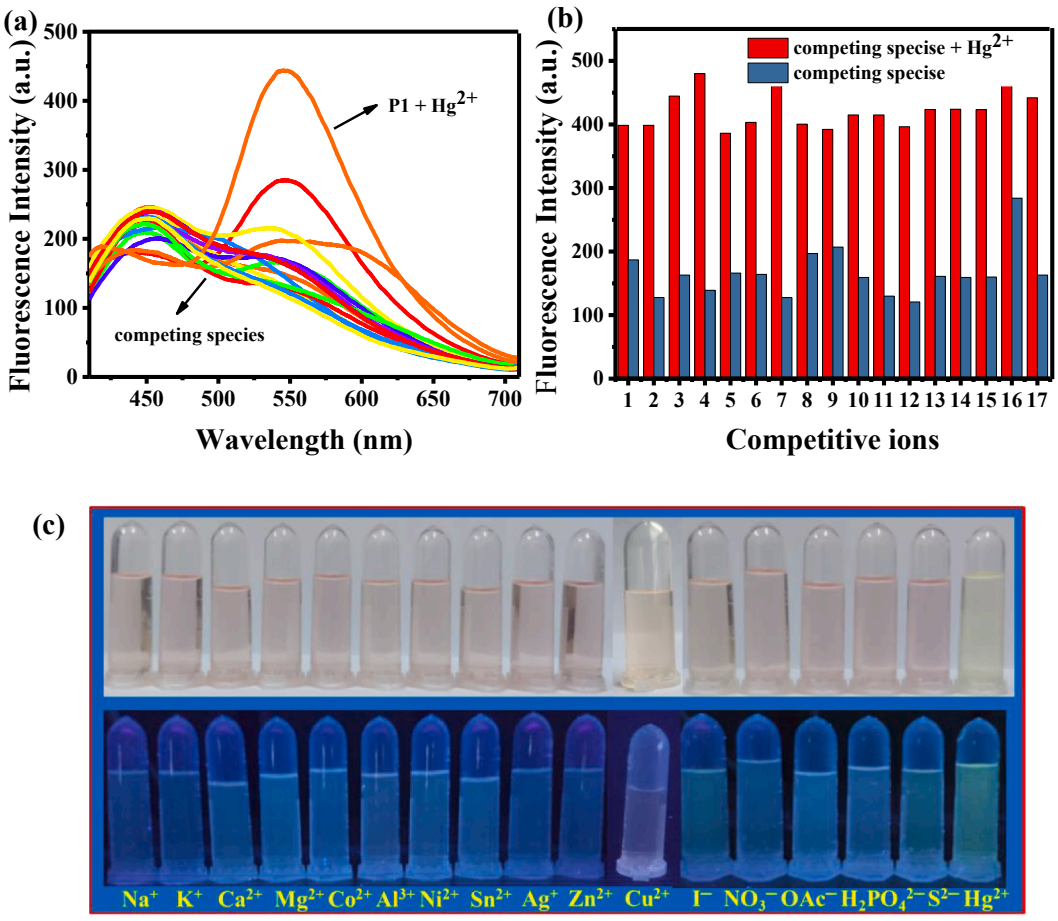

Fig. 4. (a) Fluorescent spectra of **P1** (2.5×10^{-4} M) with different competing ions (5.0×10^{-4} M) (including Na^+, K^+, Ca^{2+}, Mg^{2+}, Co^{2+}, Al^{3+}, Ni^{2+}, Sn^{2+}, Ag^{2+}, Zn^{2+}, Cu^{2+}, I^-, NO_3^-, OAc^-, $H_2PO_4^{2-}$, S^{2-}, Hg^{2+}) in CH_3OH/PBS (8:2, *v/v*, pH = 7.4, 10 mM) solution (λ_{ex} = 365 nm). (b) The fluorescence intensity of **P1** (2.5×10^{-4} M) with Hg^{2+} (5.0×10^{-4} M) in the presence of different competitive anions (5.0×10^{-4} M) in CH_3OH/PBS (8:2, *v/v*, pH = 7.4, 10 mM) solution (λ_{ex} = 365 nm). (c) Photographs of **P1** (2.5×10^{-4} M) with different competing ions (5.0×10^{-4} M) in CH_3OH/PBS (8:2, *v/v*, pH = 7.4, 10 mM) solution under day-light and 365 nm UV light.

colors of the solution changed from light red to pale yellow under daylight.

The fluorescence properties of probe **P1** were investigated. As shown in Fig. 1b, the free probe **P1** displayed two weak fluorescence emissions at 450 nm and 550 nm with excitation at 365 nm. However, upon addition of Hg^{2+}, the fluorescence intensity at around 550 nm was significantly enhanced, and the color of the solution changed from pale blue to yellow green. These results showed that the probe **P1** can serve as a colorimetric and fluorometric probe for Hg^{2+} detection.

3.2. Response time and effect of pH values of probe *P1* to Hg^{2+}

Influence of pH from 2.0 to 12.0 on the fluorescence responses of probe **P1** with and without Hg^{2+} were investigated as shown in Fig. 2a, It was known from the results of fluorescent experiments that the fluorescence emission intensities were stable in a wide pH range from 3.0 to 10.0, which indicated that the probe **P1** was suitable for detecting Hg^{2+} under the real water samples in a wide pH range. In addition, the time-dependent fluorescence results demonstrated that the probe **P1** could remain stable and recognize Hg^{2+} with a short response time (Fig. 2b).

3.3. Sensitivity of probe *P1* to Hg^{2+}

The fluorescence responses of probe **P1** to Hg^{2+} were investigated by titration experiments in CH_3OH/PBS (8:2, *v/v*, pH = 7.4, 10 mM) solution, and the results were shown in Fig. 3a. With the increasing of Hg^{2+} concentration from 0 to 2.0 equiv., the emission intensities of probe **P1** solution enhanced at 550 nm and quenched at 450 nm, which may be attributed to an ICT (intra-molecular charge transfer) process [32]. Furthermore, the emission intensities at 550 nm showed a good linear relationship over the concentration range from 0 μM to 500 μM (y = 0.5335x + 184.0493, R^2 = 0.9950). The detection limit for Hg^{2+} was calculated to be 5.4 μM based on 3σ/k method (Fig. 3b).

3.4. Selectivity and competivity of probe *P1* to various analytes

The selectivity experiments were carried out with the addition of various analytes. As shown in Fig. 4a, the fluorescence spectral changes of probe **P1** (2.5×10^{-4} M) were examined in CH_3OH/PBS (8:2, *v/v*, pH = 7.4, 10 mM) solution upon addition of different various analytes (5.0×10^{-4} M, including Na^+, K^+, Ca^{2+}, Mg^{2+}, Co^{2+}, Al^{3+}, Ni^{2+}, Sn^{2+}, Ag^{2+}, Zn^{2+}, Cu^{2+}, I^-, NO_3^-, AcO^-, $H_2PO_4^{2-}$, S^{2-}). Upon addition of these ions, there were no significant fluorescence intensity changes, while the fluorescence intensity in the presence of Hg^{2+} (5.0×10^{-4} M) obviously increased at 550 nm with the color changes from pale blue to yellow green. Meanwhile, the other competing species could hardly interfere the detection of Hg^{2+} in a complex environment (Fig. 4b). Under the day-light and 365 UV-light, the competing species did not produce any dramatic color changes and "turn-on" fluorescent emission except Hg^{2+} (Fig. 4c). The results confirmed that the probe **P1** is a specific "turn-on" fluorescent probe for detecting Hg^{2+}.

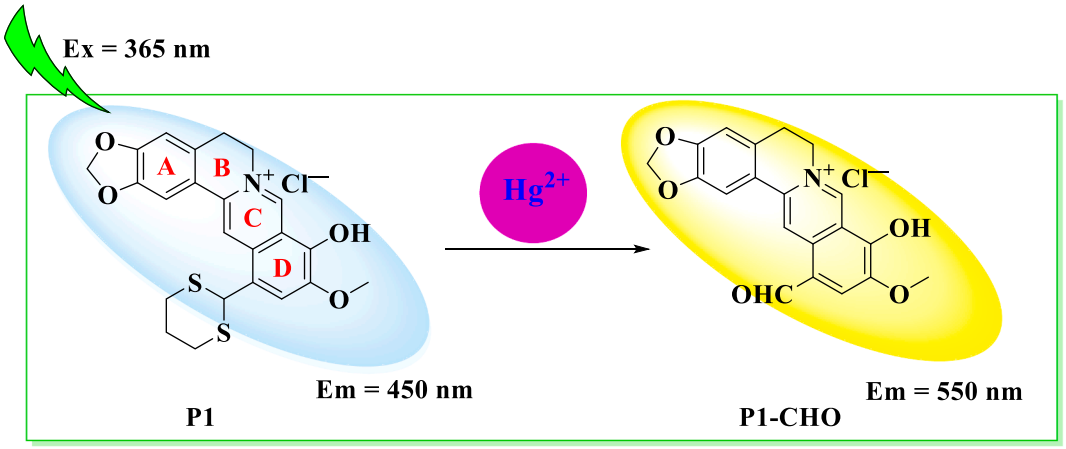

Scheme 2. Sensing mechanism of **P1**.

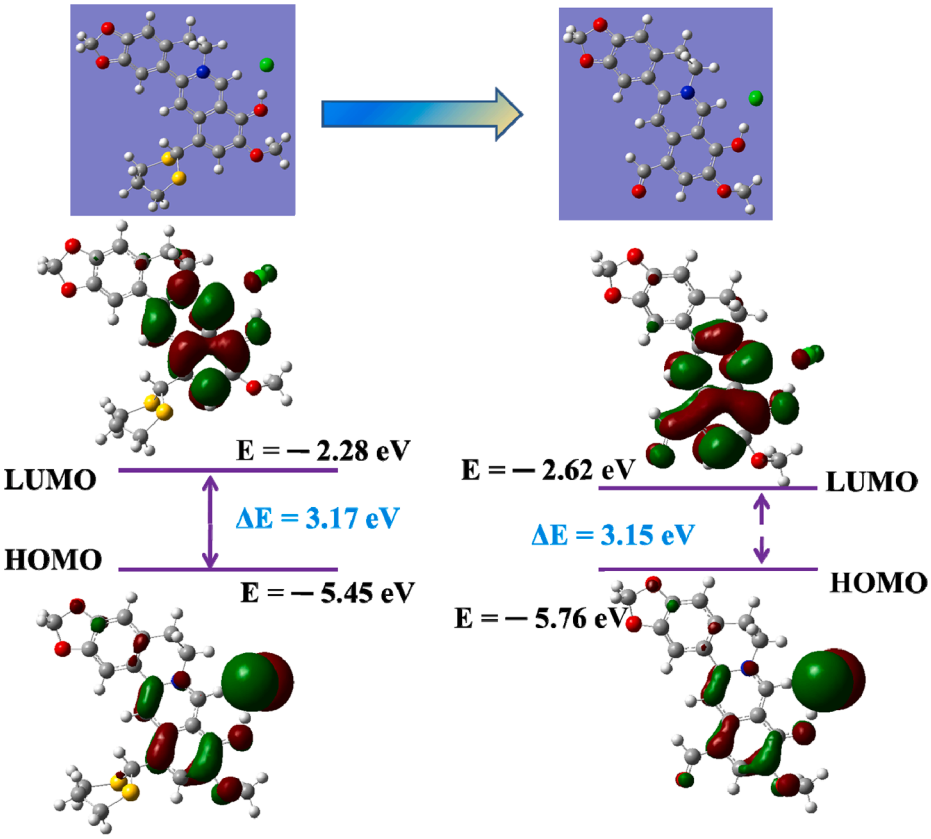

Fig. 5. The optimized geometric structures and corresponding LUMO and HOMO of **P1** and **P1-CHO** by DFT calculation.

3.5. *Sensing mechanisms of probe **P1** to Hg^{2+}*

Based on the fluorescence intensities of probe **P1** in the presence or absence of Hg^{2+}, the detection mechanism was speculated that the desulfurization reaction of probe **P1** was promoted by Hg^{2+}. The molecular ion peaks of probe **P1** before and after adding Hg^{2+} were 440.1019 [Fig. S7, P1-Cl, Exact Mass: 440.0985] and 350.1030 [Fig. S8, P1-**CHO**-Cl, Exact Mass: 350.1023]. In addition, ^{1}H NMR titration of probe **P1** with Hg^{2+} can be carried out, and these two methods indicated that detection mechanism of probe **P1** was the same with the postulated shown in Scheme 2 [33–36].

3.6. *Density functional theory (DFT) calculations*

To further understand the photophysical responses of probe **P1** to Hg^{2+}, DFT calculations were carried out with the Gaussian 09 software package. The optimized geometric structures and corresponding LUMO (the lowest unoccupied molecular orbitals) and HOMO (the highest occupied molecular orbitals) were presented. As shown in Fig. 5, the HOMO of probe **P1** was mainly localized on the hydroxyl group and part of the D ring. However, its LUMO was evenly distributed in the C and D rings, which indicated that there was a weak ICT effect in this molecule. Upon addition of Hg^{2+}, the HOMO of compound **P1-CHO** was localized on the hydroxyl group. However, the LOMO was distributed in the aldehyde group and D rings, indicating a strong ICT effect. In addition,

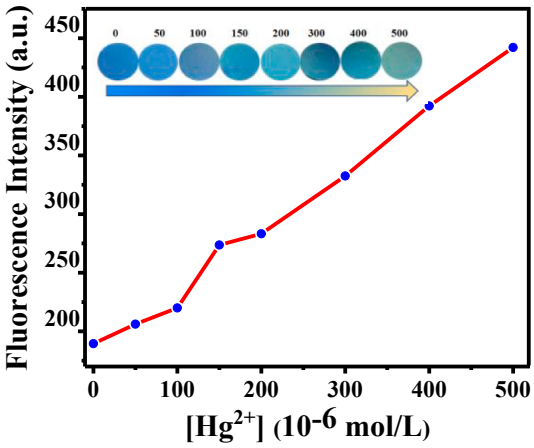

Fig. 6. Test-paper experiments of **P1** with the different concentrations of Hg^{2+} (0 μM to 500 μM).

the energy gap between HOMO and LUMO of compound **P1-CHO** was calculated to be 3.14 eV, which is lower than the probe **P1** (3.17 eV). The result also indicated that the sensing mechanism was shown in Scheme 2.

3.7. Visualization of Hg^{2+} in solution by test paper

To investigate the practical application of probe **P1** as an on-situ detection kit for the detection of Hg^{2+}, the test paper experiments were explored. As shown in Fig. 6, as the concentrations of Hg^{2+} increased from 0 μM to 500 μM, the fluorescence emission of test paper strips gradually changed from blue to faint-yellow. Therefore, the probe **P1** could successfully applied to detect Hg^{2+} on test paper.

3.8. Quantitation of Hg^{2+} contamination in real water samples

Probe **P1** could also be used to detect Hg^{2+} in two real water samples collected from Zhangjiang river and Poyang lake. The water samples were mixed with CH_3OH (80%) solutions containing the probe **P1** (2.5×10^{-4} M). The various concentrations of Hg^{2+} solution (0, 50, 100, 150, 200, 250 μM) were added into experimental water samples respectively. The fluorescence intensity of the experimental samples was measured using a fluorescence spectrophotometer. As shown in Fig. 7, two good linear relationships were obtained, and the detection limit for Hg^{2+} was calculated to be 6.3 μM and 4.4 μM, indicating that the probe **P1** can be applied to detect Hg^{2+} in real samples.

4. Conclusion

In summary, the probe **P1** for detecting Hg^{2+} was synthesized from berberine. This probe could identify Hg^{2+} in CH_3OH/PBS (8:2, *v/v*, pH = 7.4, 10 mM) solution by the obvious color changes at daylight and the perfect fluorescence changes under 365 nm UV lamp. The probe **P1** displayed high selectivity, superior sensitivity, and fast response toward Hg^{2+} with a low detection limit and a wide pH range. The probe **P1** can provide a convenient and effective way for Hg^{2+} detection by virtue of test paper strips. Moreover, this probe can be also applied to monitor Hg^{2+} in real environmental water samples.

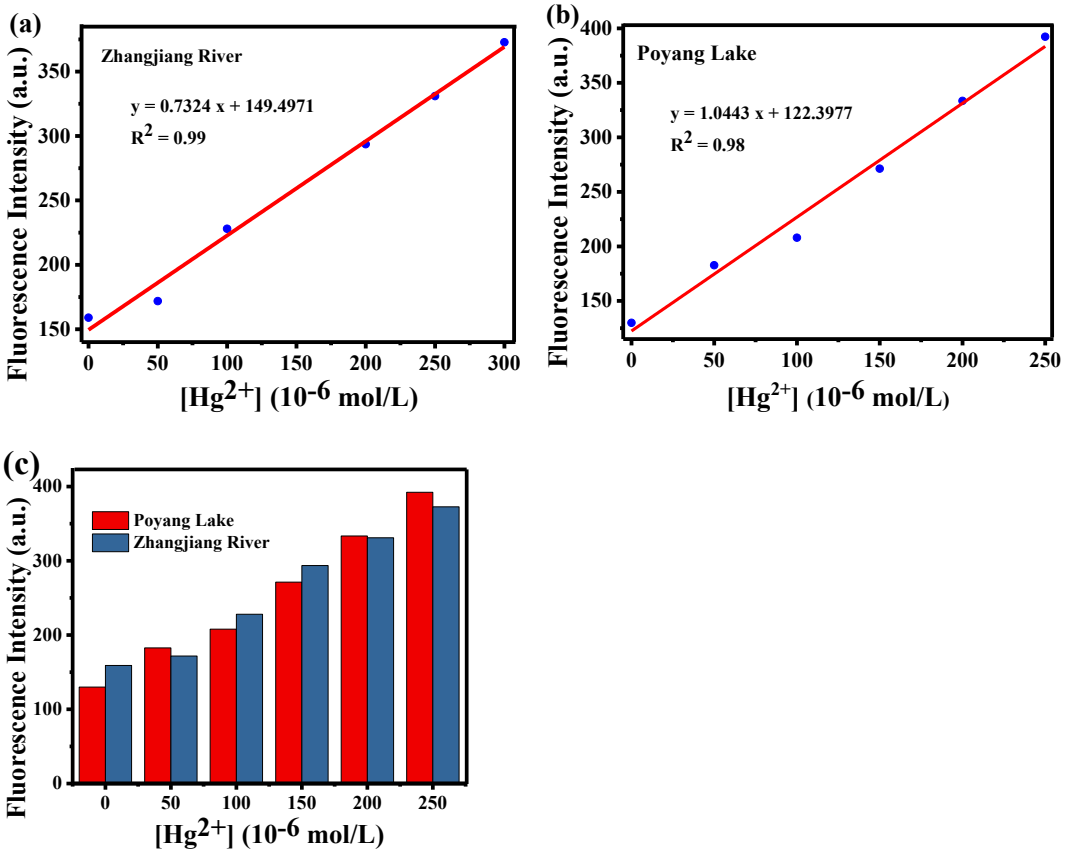

Fig. 7. (a) The linear relationship of fluorescence intensity of **P1** and different concentrations of Hg^{2+} in Zhangjiang river (λ_{em} = 550 nm). (b) The linear relationship of fluorescence intensity of **P1** and different concentrations of Hg^{2+} in Poyang lake (λ_{em} = 550 nm). (c) The fluorescence intensity of **P1** (2.5×10^{-4} M) towards different concentration of Hg^{2+} (0, 50, 100, 150, 200, 250 μM) (λ_{em} = 550 nm).

CRediT authorship contribution statement

Shutang Ruan: Conceptualization, Data curation, Methodology, Writing – original draft. **Yan Zhang:** Formal analysis, Resources. **Suzhen Wu:** Investigation. **Yu Gao:** Investigation. **Lijuan Yang:** Resources. **Mingxin Li:** Software. **Yiqin Yang:** Supervision. **Zhonglong Wang:** Writing – review & editing. **Shifa Wang:** Funding acquisition, Project administration.

Declaration of Competing Interest

The authors declare that they have no known competing financial interests or personal relationships that could have appeared to influence the work reported in this paper.

Acknowledgements

This research was supported by the National Natural Science Foundation of China (No. 32071707).

Appendix A. Supplementary material

Supplementary data to this article can be found online at https://doi.org/10.1016/j.inoche.2021.108847.

References

[1] E.M. Nolan, S.J. Lippard, Tools and Tactics for the Optical Detection of Mercuric Ion, Chem. Rev. 108 (2008) 3443–3480.
[2] H.H. Harris, I.J. Pickering, G.N. George, The chemical form of mercury in fish, Science 301 (2003) 1203.
[3] A. Renzoni, F. Zino, E. Franchi, Mercury levels along the food chain and risk for exposed populations, Environ. Res. 77 (1998) 68–72.
[4] S.M. Shenawy, N.S. Hassan, Comparative evaluation of the protective effect of selenium and garlic against liver and kidney damage induced by mercury chloride in the rats, Pharmacol. Rep. 60 (2008) 199–208.
[5] M. Harada, Minamata disease, methylmercury poisoning in Japan caused by environmental pollution, Journal Critical Reviews in Toxicology 25 (1) (1995) 1–24.
[6] F.D. Natale, A. Lancia, A. Molino, M. Di Natale, D. Karatza, D. Musmarra, Capture of mercury ions by natural and industrial materials, J. Hazard. Mater. 132 (2006) 220–225.
[7] M. Vedamalai, D. Kedaria, R. Vasita, S. Moric, I. Gupta, Design and synthesis of BODIPY-clickate based Hg^{2+} sensors: the effect of triazole binding mode with Hg^{2+} on signal transduction, Dalton Trans. 45 (2016) 2700–2708.
[8] Z.e. Wu, X. Feng, P. Li, C.-J. Lin, G. Qiu, X. Wang, H. Zhao, H. Dong, Comparison of in vitro digestion methods for determining bioaccessibility of Hg in rice of China, J. Environ. Sci. 68 (2018) 185–193.
[9] A.F. Danet, M.C. Bratu, M.C. Radulescu, A. Bratu, Portable minianalyzer based on cold vapor atomic absorption spectrometry at 184.9 nm for atmospheric mercury determination, Sens. Actuators, B 137 (2009) 12–16.
[10] A.T. Townsend, K.A. Miller, S. McLean, S. Aldous, The determination of copper zinc, cadmium and lead in urine by high resolution ICP-MS, J. Anal. At. Spectrom. 13 (11) (1998) 1213–1219.
[11] M.S. Hosseini, H.H. Moghaddam, Sensitized extraction spectrophotometric determination of Hg (II) with dithizone after its flotation as ion-associate using iodide and ferroin, Talanta 67 (2005) 555–559.
[12] Z. Ma, Y. Sun, J. Xie, P. Li, Q. Lu, M. Liu, P. Yin, H. Li, Y. Zhang, S. Yao, Facile Preparation of MnO2 Quantum Dots with Enhanced Fluorescence via Microenvironment Engineering with the Assistance of Some Reductive Biomolecules, ACS Appl. Mater. Interfaces 12 (13) (2020) 15919–15927.
[13] Z.Y. Ma, T.T. Wu, P.P. Li, M.L. Liu, S. Huang, H.T. Li, Y.Y. Zhang, S.Z. Yao, A dual (colorimetric and fluorometric) detection scheme for glutathione and silver (I) based on the oxidase mimicking activity of MnO_2 nanosheets, Microchim Acta 186 (2019) 498.
[14] L.Q. Yang, N. Huang, L.Y. Huang, M.L. Liu, H.T. Li, Y.Y. Zhang, S.Z. Yao, An electrochemical sensor for highly sensitive detection of copper ions based on a new molecular probe Pi-A decorated on grapheme, Anal. Methods 9 (2017) 618–624.
[15] A. Fang, H. Chen, H. Li, M. Liu, Y. Zhang, S. Yao, Glutathione regulation-based dual-functional upconversion sensing-platform for acetylcholinesterase activity and cadmium ions, Biosens. Bioelectron. 87 (2017) 545–551.
[16] F. Ru, P. Du, X. Lu, Efficient ratiometric fluorescence probe utilizing silicon particles/goldnanoclusters nanohybrid for "on-off-on" bifunctional detection and cellular imaging of mercury (II) ions and cysteine, Anal. Chim. Acta 1105 (2020) 139–146.
[17] X.M. Wu, Y.N. Li, S.X. Yang, H.Y. Tian, B.G. Sun, A multiple-detection-point fluorescent probe for the rapid detection of mercury(II), hydrazine and hydrogen sulphide, Dyes Pigm. 174 (2020), 108056.
[18] S. Lal, K. Prakash, N. Khera, S. Drashya, A. Singh, S. Singh, R.C. Hooda, Curcumin based supramolecular ensemble for optical detection of Cu^{2+} and Hg^{2+} ions, J. Mol. Struct. 1211 (2020), 128091.
[19] Q. Su, Q. Niu, T. Sun, T. Li, A simple fluorescence turn-on chemosensor based on Schiff-base for Hg2+-selective detection, Tetrahedron Lett. 57 (38) (2016) 4297–4301.
[20] W. Ma, Q. Xu, J. Du, B.o. Song, X. Peng, Z. Wang, G. Li, X. Wang, A Hg^{2+}-selective chemodosimeter based on desulfurization of coumarin thiosemicarbazide in aqueous media, Spectrochim. Acta, Part A 76 (2) (2010) 248–252.
[21] H. Lin, W. Shi, Y. Tian, F. Ma, L. Xu, J. Ma, Y. Hui, Z. Xie, A simple and highly selective 'turn-on' type fluorescence chemodosimeter for Hg^{2+} based on 1-(2-phenyl-2H-[1,2,3]triazole-4-carbonyl) thiosemicarbazide, J. Lumin. 157 (2015) 280–284.
[22] L. Yang, Y.A. Su, Y.N. Geng, H.Q. Xiong, J.L. Han, Q. Fang, X.Z. Song, A red-emitting fluorescent probe for detecting Hg^{2+} in aqueous medium, living cells and organism with a large Stokes shift, Org. Biomol. Chem. 16 (2018) 5036–5042.
[23] A.W. Baird, C.T. Taylor, D.J. Brayden, Non-antibiotic anti-diarrhoeal drugs: factors affecting oral bioavailability of berberine and loperamide in intestinal tissue, Adv. Drug Deliv. Rev. 23 (1997) 111–120.
[24] C. Chen, Z.M. Luo, H.J. Yang, Y.C. Feng, A novel synthetic route for berberine chloride, Chin. J. Chem . 36 (2016) 1426–1430.
[25] K. Iwasa, D.U. Lee, S.I. Kang, W. Wiegrebe, Antimicrobial activity of 8-alkyl- and 8-phenyl-substituted berberines and their 12-bromo derivatives, J. Nat. Prod. 61 (1998) 1150–1153.
[26] T. Li, P.L. Wang, W.B. Guo, X.M. Huang, X.H. Tian, G.R. Wu, B. Xu, F.F. Li, C. Yan, X.J. Liang, H.M. Lei, Natural berberine-based Chinese herb medicine assembled nanostructures with modified antibacterial application, ACS Nano 13 (2019) 6770–6781.
[27] Y.X. Liu, C.L. Xiao, Y.X. Wang, Y.H. Li, Y.H. Yang, Y.B. Li, C.W. Bi, L.M. Gao, J. D. Jiang, D.Q. Song, Synthesis, structure activity relationship and in vitro anti-mycobacterial evaluation of 13-*n*-octylberberine derivatives, Eur. J. Med. Chem. 52 (2012) 151–158.
[28] K. Hauashi, K. Minoda, Y. Nagaoka, Antiviral activity of berberine and related compounds against human cytome-galovirus, Bioorg. Med. Chem. Lett. 17 (2007) 1562–1564.
[29] H.S. Bodiwala, S. Sabde, D. Mitra, K.K. Bhutani, I.P. Singh, Synthesis of 9-substituted derivatives of berberine as anti-HIV agents, Eur. J. Med. Chem. 46 (2011) 1045–1049.
[30] M.M.S. Lee, L. Zheng, B. Yu, W. Xu, R.T.K. Kwok, J.W.Y. Lam, F. Xu, D. Wang, B. Z. Tang, A highly efficient and AIE-active theranostic agent from natural herbs, Mater. Chem. Front. 3 (7) (2019) 1454–1461.
[31] S.T. Ruan, S.Z. Wu, L.J. Yang, M.X. Li, Y. Zhang, Z.L. Wang, S.F. Wang, A novel turn-on fluorescent probe based on berberine for detecting Hg^{2+} and ClO^{-} with the different fluorescence signals, Microchem. J. 66 (2021), 106199.
[32] Y. Gao, T. Ma, Z. Ou, W. Cai, G. Yang, Y.i. Li, M. Xu, Q. Li, Highly sensitive and selective turn-on fluorescent chemosensors for Hg^{2+} based on thioacetal modified pyrene, Talanta 178 (2018) 663–669.
[33] P.C. Yin, Q.F. Niu, Q.X. Yang, L.X. Lan, T.D. Li, A new "naked-eye" colorimetric and ratiometric fluorescent sensor for imaging Hg^{2+} in living cells, Tetrahedron 75 (2019), 130687.
[34] X. Li, Q. Duan, Y. Yu, K. Wang, H. Zhu, X. Zhang, C. Liu, P. Jia, Z. Li, W. Sheng, B. Zhu, A coumarin-based fluorescent probe for Hg^{2+} and its application in living cells and zebrafish, Luminescence 35 (6) (2020) 941–946.
[35] D. Xu, L. Tang, M. Tian, P. He, X. Yan, A benzothizole-based fluorescent probe for Hg^{2+} recognition utilizing ESIPT coupled AIE characteristics, Tetrahedron Lett. 58 (37) (2017) 3654–3657.
[36] Y.Y. Liu, S. Naha, N. Thirumalaivasan, S. Velmathi, S.P. Wu, A novel nanomolar highly selective fluorescent probe for imaging mercury (II) in living cells and zebrafish, Sens. Actuators, B 277 (2018) 673–678.